Analyst

PAPER

View Article Online
View Journal

Cite this: DOI: 10.1039/d6an00592f

Dual-readout villus-like scaffold microfluidic platform for quantitative analysis of gut microbiota formation under perfusion

Yota Yamakawa,[a,b] Ryoo Hidaka,[a] Wataru Iwasaki,[b,c] Sachiko Ide[a] and Noritada Kaji *[a,d]

A dual-readout modular microfluidic platform integrating a villus-like scaffold is presented for quantitative analysis of bacterial colonization and functional outputs under perfusion. The gut microbiota plays pivotal roles in host immunity and metabolism, and its assembly is strongly influenced by the order of bacterial arrival and colonization in the intestinal tract. To quantitatively investigate microbiota formation, an analytical system that unifies a three-dimensional (3D) microenvironment with fluidic transport and multimodal readouts is required. Here, we develop a villus-like scaffold-integrated modular microfluidic device enabling dual readout: (i) *in situ* fluorescence imaging and quantification of bacterial attachment on the scaffold, and (ii) effluent biochemical assays for metabolic and functional outputs. The villus-like scaffold was fabricated by replica molding using an acrylic master and polydimethylsiloxane (PDMS) molds, where ultrasonication-assisted bubble removal and post-gelation dehydration in 99% ethanol improved structural replication. The fabricated villus-like agarose scaffold showed a replication yield of up to 100%, with pillar dimensions of 192.1 ± 2.4 μm in diameter and 522.0 ± 10.3 μm in height. Under perfusion at 32 μL min^{-1}, the 3D scaffold increased *L. plantarum* colonization and lactate production compared with the flat hydrogel control, while *E. coli* exhibited increased scaffold-localized fluorescence despite decreased effluent β-glucuronidase (GUS) signals over 8 h. This device-oriented system integrates villus-like scaffold architecture, perfusion operation, and dual-readout quantification, providing a scalable foundation for analytical studies of gut microbiota assembly.

Received 21st May 2026,
Accepted 25th May 2026

DOI: 10.1039/d6an00592f

rsc.li/analyst

Introduction

The human gastrointestinal tract hosts a diverse microbial community that profoundly impacts host physiology, including immune and metabolic regulation.[1,2] Dysbiosis, *i.e.*, altered microbiota composition, has been associated with a wide range of diseases[3] and resilience.[4] Importantly, the assembly process of gut microbial communities is not solely dictated by external factors such as diet and lifestyle but is also influenced by the order of microbial arrival and colonization, as well as colonization resistance exerted by established communities.[5]

Current microbiome studies often rely on fecal sampling combined with sequencing-based profiling. While powerful, fecal microbiome composition does not always represent site-specific colonization in the gut,[6,7] making it difficult to resolve the spatial and temporal processes underlying community formation. Animal models provide valuable insights but are constrained by ethical considerations and interspecies differences. Accordingly, there is growing demand for *in vitro* analytical platforms that allow controlled observation and quantification of bacterial colonization and functional outputs under physiologically relevant microenvironments.[8–10]

Microfluidic organ-on-a-chip systems have emerged as promising tools to emulate tissue microenvironments by controlling fluid flow, chemical gradients, and micro-scale geometry.[11–14] In parallel, 3D hydrogel scaffolds that mimic intestinal villi have been developed to reproduce high-aspect-ratio architectures.[15–18] However, many reported villus-mimicking systems prioritize epithelial tissue reconstruction, and fewer studies have focused on device-driven quantitative analysis of bacterial attachment and metabolic functions. Because microenvironmental features—such as surface topography and transport

[a]Department of Applied Chemistry, Graduate School of Engineering, Kyushu University, Fukuoka 819-0395, Japan. E-mail: kaji@cstf.kyushu-u.ac.jp; Tel: +81-92-802-2883
[b]Sensing Technology Research Institute, National Institute of Advanced Industrial Science and Technology, Tosu 841-0052, Japan
[c]Integrated Research Center for Wellbeing, National Institute of Advanced Industrial Science and Technology, Tosu 841-0052, Japan
[d]Institute of Nano-Life-Systems, Institutes of Innovation for Future Society, Nagoya University, Nagoya 464-8603, Japan

conditions though mucin layer—are critical determinants of bacterial colonization,[19] there remains a need for a device-centric analytical system integrating (i) a villus-like 3D scaffold coated by mucin layer, (ii) robust perfusion operation, and (iii) quantitative readouts combining imaging and biochemical assays.

In this work, we developed a villus-mimicking hydrogel scaffold covered with porcine gastric mucin layer–integrated modular microfluidic device for bacterial cultivation and quantification. Porcine gastric mucin (PGM) serves as a robust and highly effective *in vitro* model for human gastric mucin (HGM), primarily due to its substantial homology in core protein architecture and macroscopic physicochemical properties. Recent biomacromolecular studies demonstrate that the MUC5AC-driven gelation mechanisms and cross-linking networks are fundamentally conserved, validating PGM's structural utility.[20] Furthermore, advanced macrorheological and tribological characterizations confirm that PGM accurately replicates the shear-thinning, viscoelasticity, and lubricating behaviors of native human gastrointestinal mucus at soft interfaces.[21] However, researchers must carefully account for discrepancies in glycosylation. While PGM shares critical terminal O-glycan epitopes necessary for baseline biomolecular interactions, mass spectrometric analyses reveal diverse oligosaccharide profiles and significant individual glycan variations.[22] Therefore, PGM stands as an exceptionally reliable physical and structural surrogate for engineered platforms—such as microfluidic assays and bio-interfaces proved that highly specific, glycan-mediated recognition events are rigorously calibrated.[18] The platform was designed as a next-generation analytical system featuring two complementary readouts: software-based *in situ* fluorescence quantification on the scaffold and effluent analysis for bacterial metabolic and functional markers. Conventional effluent analysis alone cannot distinguish between "colonization" and "wash-out", which poses a risk of misinterpretation. For example, it may appear that bacteria levels have decreased when, in reality, colonization has not occurred. This device resolves this ambiguity by incorporating imaging analysis. We validated the platform using *L. plantarum* and *E. coli* under both static and dynamic conditions and demonstrated scaffold-enhanced colonization and metabolic outputs under perfusion.

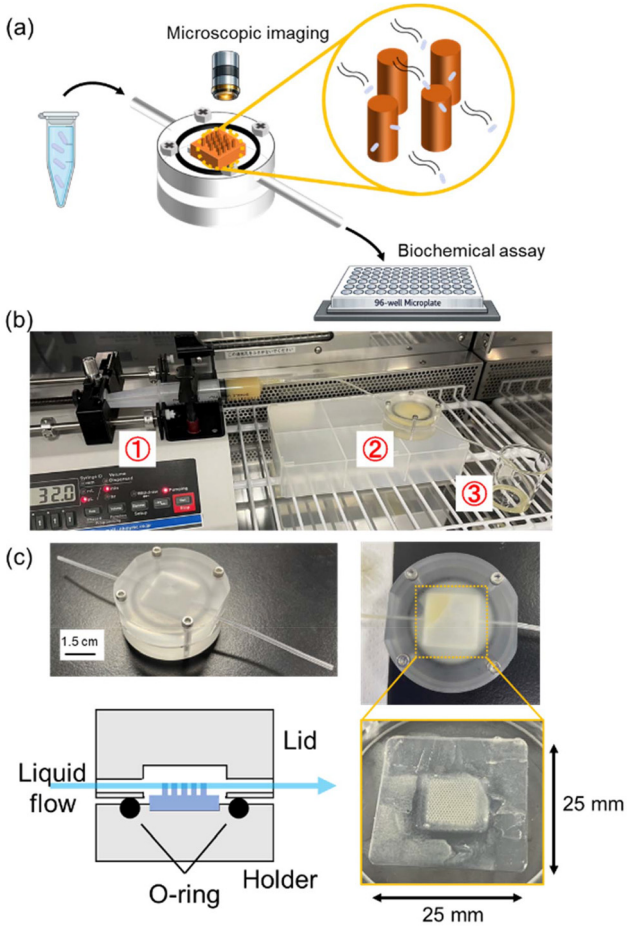

Fig. 1 Overview of the villus-mimicking scaffold-integrated modular microfluidic platform enabling dual readouts. (a) Conceptual schematic illustrating *in situ* fluorescence imaging on the 3D scaffold and effluent collection for biochemical quantification. (b) Photograph of the device setup showing the scaffold chamber, O-ring sealing, screw fixation, syringe pump, and inlet/outlet ports. (c) Photographs of the modular microfluidic device and the cross-sectional image. The embedded scaffold inside the scaffold chamber was immobilized with agarose and sealed with a lid, and filled with the medium through the connected tube.

Materials and methods

Device architecture and fabrication

A modular microfluidic device was designed to accommodate a villus-mimicking hydrogel scaffold in a sealed chamber as shown in Fig. 1. The device consisted of an acrylic holder and an acrylic lid. The holder contained a central scaffold chamber (25 mm × 25 mm × 1 mm). An O-ring groove (outer diameter 44 mm, inner diameter 38 mm, depth 1.5 mm) surrounded the chamber to ensure reliable sealing. Four M3 screw holes were placed outside the groove. The lid featured a corresponding cavity (25 mm × 25 mm × 3 mm), four M3 screw holes, and two through-holes (1.3 mm in diameter) for tubing connections. Both components were fabricated *via* acrylic machining.

For assembly, the 3D scaffold was placed in the central chamber. The peripheral gap around the scaffold was filled with molten 2% agarose and allowed to gelation at room temperature, immobilizing the scaffold. An O-ring was inserted, and the device was tightened using M3 screws. Polyethylene tubes (outer diameter 1.3 mm) were connected to the device and the other ends were connected to silicone tubes (inner diameter 1.02 mm) for syringe pump connection and the liquid drain, respectively. A flat agarose scaffold without villus structures was prepared as a control.

Fabrication of villus-mimicking 3D hydrogel scaffolds

An acrylic master mold with an array of cylindrical holes was designed using CAD (AutoCAD, Autodesk, Inc., Tokyo, Japan) and fabricated using a desktop micro-machining system

(Micro MC-2, PMT corporation, Fukuoka, Japan). The design parameters were: hole diameter 200 μm, pitch 300 μm, and depth 500 μm. PDMS (SILPOT 184, DuPont Tokyo Specialty Materials K. K., Tokyo, Japan) and curing agent were mixed at a 6 : 1 weight ratio, degassed, poured onto the master mold, and cured at 65 °C for 12 h to obtain a positive PDMS mold. The PDMS surface was silanized to facilitate demolding, and a negative PDMS mold was also fabricated.

Molten 2% agarose solution was poured into the negative mold. To improve filling into micro-holes, the mold was treated with ultrasonication to remove trapped air bubbles. After gelation, the mold containing the agarose scaffold was immersed in 99% ethanol overnight. Dehydration process of agarose gel accelerated the slight shrinkage of the agarose replica without changing the designed structure and facilitated demolding easier. Structural replication yield was evaluated as the number of successfully formed villus structures divided by the number of designed holes in the master mold.

Bacterial culture

L. plantarum JCM1149 and *E. coli* JM109 were used as model bacteria. *L. plantarum* was cultured in MRS medium (Merck, Darmstadt, Germany), and *E. coli* was cultured in LB medium (BD Biosciences, Tokyo, Japan) at 37 °C. Colonies were obtained on agar plates, and bacterial suspensions were prepared by shaking culture.

Static colonization assay and imaging-based quantification

To mimic a mucus layer, mucin from porcine stomach (Fujifilm, Tokyo, Japan) was dissolved to 20 mg mL^{-1} and sterilized at 60 °C for 1 h. The hydrogel scaffold was immersed in mucin solution overnight. A bacterial suspension was inoculated onto the scaffold and incubated at 37 °C. For single-species imaging, nucleic acids were stained using Cellstain AO (Acridine Orange) (FUJIFILM Corporation, Tokyo, Japan) and the fluorescence images were acquired by confocal microscope (TCS SP8, Leica, Tokyo, Japan). The fluorescence intensities of the surface of the villus-like structures were analyzed by ImageJ (NIH) and used as a metric of bacterial attachment.

For dual-species visualization, *L. plantarum* and *E. coli* were labeled with SYTO 85 (ThermoFisher Scientific, Tokyo, Japan) and Hoechst 33342 (ThermoFisher Scientific), respectively, enabling multiplexed fluorescence imaging.

Dynamic perfusion culture and effluent biochemical assays

For perfusion experiments, bacterial suspensions (10^9 CFU mL^{-1}) in LB medium were mixed with the mucin solution to yield 10^8 CFU mL^{-1}. The mixture was loaded into a 20 mL syringe and infused using a syringe pump. The flow rate was set to 32 μL min^{-1} to emulate physiologically relevant flow velocity.[23–25] Effluent samples were collected at 2, 4, and 8 h (1 h collection for each time point).

For *L. plantarum* assays, lactate concentration was measured using a colorimetric kit (FUJIFILM Corporation, Tokyo, Japan) based on WST-formazan formation. Supernatants of the collected effluent were diluted 20-fold, reacted at 37 °C for 30 min, and absorbance at 450 nm was recorded. For *E. coli* assays, β-glucuronidase (GUS) activity was measured fluorometrically using 4-methylumbelliferyl-β-D-glucuronide (MUG) substrate.[26] After incubation at 37 °C for 20 min, fluorescence was recorded at E_x 360 nm/E_m 450 nm.

For co-culture experiments, *L. plantarum* and *E. coli* were mixed at a 1 : 1 concentration ratio (total 10^8 CFU mL^{-1}) and analyzed using both lactate and GUS readouts.

Results and discussion

The proposed platform was designed as a device-oriented analytical system rather than a tissue reconstruction model. It combined (i) a villus-like 3D hydrogel scaffold offering high-aspect-ratio microtopography, (ii) a robust modular microfluidic chamber enabling stable perfusion, and (iii) two complementary quantification routes: *in situ* fluorescence imaging and effluent biochemical analysis of metabolic/functional outputs. This integration provided a practical foundation for quantitative studies of bacterial colonization under transport conditions relevant to the gut.

Replicable fabrication of a villus-like scaffold: process optimization and geometric fidelity

A key requirement for a device-oriented analytical platform is a reproducible scaffold component with controlled microtopography. As shown in Fig. 2, the acrylic master mold yielded microhole geometries close to the designed values (diameter ~207 μm, pitch ~497 μm, depth ~514 μm), confirming that the machining process provided sufficient fidelity for subsequent replica molding. During agarose casting into the negative PDMS mold, incomplete filling was initially observed, indicating that trapped air bubbles limited agarose penetration into the microcavities. Introducing ultrasonication during casting effectively removed bubbles and improved filling into the cavities. Post-gelation immersion in 99% ethanol further increased the replication yield and reduced variability, with longer immersion times producing higher yields. This improvement was attributed to dehydration-induced densification and strengthening of the gel, which facilitated demolding and preserved microstructures. As a result, villus-like microstructures with representative dimensions of 192.1 ± 2.4 μm in diameter and 522.0 ± 10.3 μm in height were obtained, corresponding to an aspect ratio of ~2.72; the aspect ratio did not substantially change after incubation in an incubator, indicating sufficient structural stability for the following cultivation experiments. Collectively, ultrasonication for void removal and ethanol immersion for gel densification and yield improvement established a controllable fabrication window for producing villus-like scaffolds as device components rather than one-off biomimetic constructs.

Static colonization assay as a quantitative imaging benchmark: dependence on inoculation density and incubation time

To convert scaffold colonization into a quantitative readout, fluorescence images were evaluated under static conditions as

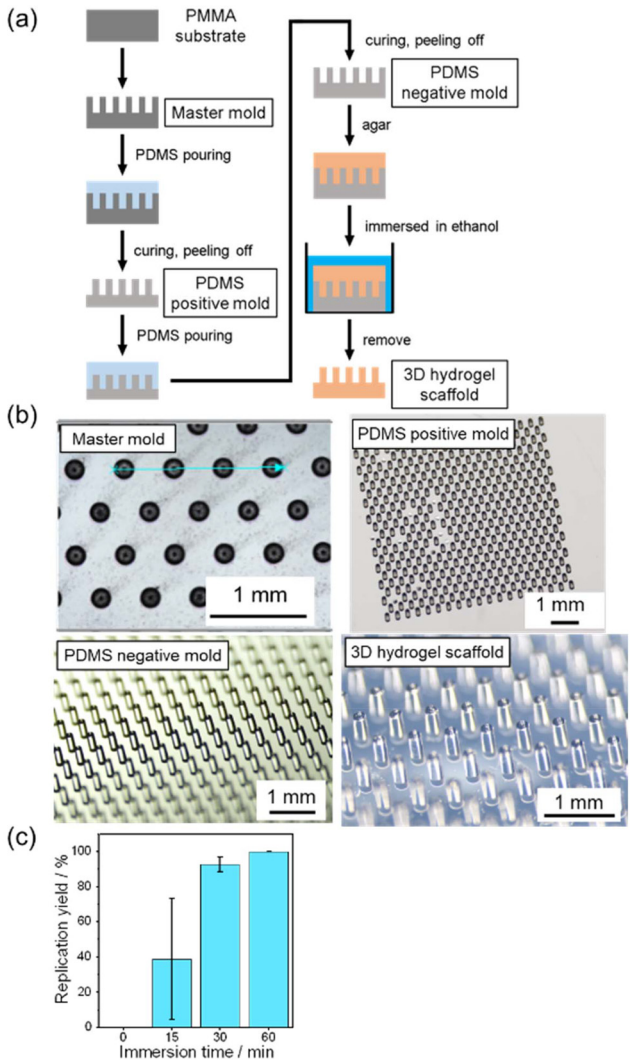

Fig. 2 The fabrication workflow and replication performance of the villus-mimicking 3D hydrogel scaffold are presented. (a) Replica-molding procedure using an acrylic master mold, PDMS molds, and agarose casting. The dimensions of the master mold are as follows: diameter: 200 μm; pillar-to-pillar distance: 300 μm; height: 500 μm. (b) Representative images of the fabricated structures taken under a stereomicroscope. (c) Replication yield as a function of ethanol immersion time to remove the final 3D hydrogel scaffold from the PDMS positive mold (n = 295).

shown in Fig. 3. Increasing the inoculation density resulted in higher fluorescence intensity for both *L. plantarum* and *E. coli*, supporting the use of fluorescence intensity-based metrics as a proxy for bacterial abundance on the scaffold. Similarly, extending the incubation time increased fluorescence intensities, indicating that both species could attach and grow on the villus-like agarose structures in a mucus-mimicking environment. Based on intensity changes, the estimated doubling times were approximately 3.78 h for *L. plantarum* and 4.77 h for *E. coli*, suggesting that mucin alone may provide limited nutrients compared with nutrient-rich media and thus lead to slower growth. In addition, *L. plantarum* tended to show higher fluorescence intensities than *E. coli* under comparable conditions, which could potentially relate to a difference in dye permeability associated with Gram-negative outer membranes.

For two-species visualization, spectral overlap between SYTO 85 and acridine orange (AO) complicated population discrimination, prompting an optimized labeling scheme. Introducing Hoechst 33342 improved separability and enabled species-specific observation on the scaffold. Under mixed inoculation with varied ratios, the attachment of both populations was confirmed. This demonstrates the feasibility of multi-species colonization assays on the villus-like scaffold under static conditions, though quantitation requires improvement (Fig. S1 and S2).

These results establish the static assay as a calibration step: fluorescence imaging-based quantification provides a practical software-enabled metric for scaffold-localized colonization and supports extension to multi-species readouts through appropriate dye design.

Dynamic perfusion cultivation: dual readout reveals villus-structure effects and transport-dependent signatures

The modular device enabled dynamic perfusion experiments with defined sampling (2, 4, and 8 h) and flow operation, allowing time-resolved effluent analytics while maintaining the capability for imaging-based evaluation of scaffold-localized colonization. As shown in Fig. 4(a) and (b), lactate concentrations in effluent samples increased with cultivation time under perfusion, demonstrating active metabolism of *L. plantarum* within the device. Viable counts increased up to 2 h on the flat scaffold and up to 4 h on the villus-like scaffold, followed by a decrease at later time points, consistent with growth inhibition likely caused by acidification (low pH) during lactate accumulation. Notably, viable counts were higher on the villus-like scaffold than on the flat control across the tested conditions, supporting the interpretation that the villus-like microtopography promotes retention and/or attachment, thereby enhancing effective colonization under flow. This scaffold effect is a central device-level finding: the same flow operation produces different cultivation outcomes depending on scaffold architecture, highlighting the analytical value of incorporating villus-like structures.

For *E. coli*, both GUS activity estimated by the effluent fluorescence and viable counts in the collected effluent decreased over time. This behavior differed from the initial expectation of monotonic increase. Importantly, despite decreasing effluent-based signals, fluorescence imaging on the scaffold showed increasing intensities with perfusion time, indicating that colonization and growth within the device progressed locally on the scaffold surfaces (Fig. 4(d) and (e)). The cause of this contradictory situation might be the *E. coli* deviation from the solution flow within the device and drifted around inside the device. The average swimming velocity of *E. coli* JM109 *via* flagella, the strain used in this study, has been reported to be 5.93 μm s^{-1},[27] the flow velocity within the device—assuming the culture medium flows uniformly inside the device—is

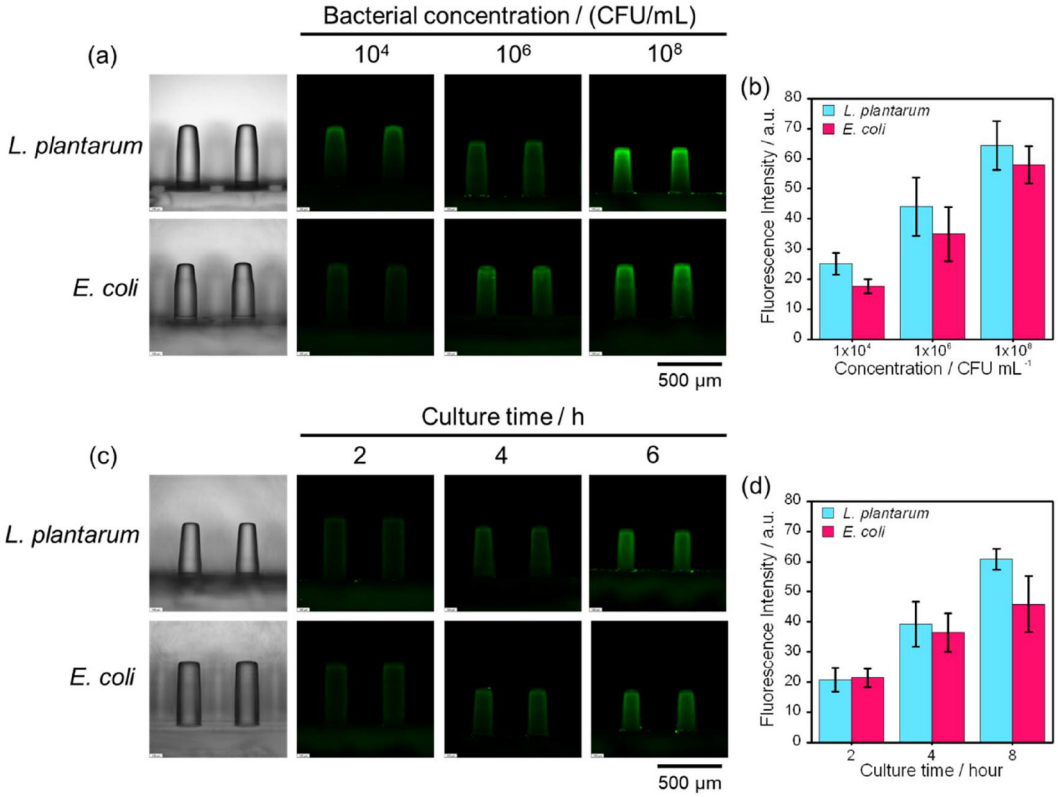

Fig. 3 Representative cross-sectional images of the 3D hydrogel scaffold were captured by a confocal microscope at the bacterial concentrations and culture times indicated above the images (a and c). The quantitative analysis of the fluorescence intensity of bacteria stained with Cellstain AO attached to the pillars is shown as a function of (b) the initial bacterial concentration at a culture time of 2 hours and (d) the culture time at an initial bacterial concentration of 10^8 CFU mL^{-1}. The fluorescence intensities and error bars represent the mean and standard deviation of 12 pillar images, respectively.

7.11 μm s^{-1}. This suggests that the part of *E. coli* may have drifted out of the main flow or swimming against the flow of the solution within the device and were floating or sinking within it. If there were a metabolite specific to *E. coli* that is excreted into the environment, similar to the lactic acid produced by *L. plantarum*, the current issues could be resolved. This divergence between effluent readout and *in situ* imaging underscores the need for dual readout: relying on effluent measurements alone may underestimate scaffold-localized colonization, whereas imaging alone cannot quantify functional outputs in the outflow. The combined readout clarifies that transport and localized growth can yield opposing signatures, a phenomenon that becomes interpretable only when both readouts are available.

Co-culture under perfusion for microbiota formation analysis

To take a step toward quantitative analysis of microbiota formation, we performed co-culture experiments of *L. plantarum* and *E. coli* under continuous perfusion and evaluated the system using effluent analytical readouts. Under co-culture, the effluent lactate concentration on the villus-like scaffold increased with perfusion time, and the difference relative to the flat scaffold control became more pronounced at 8 h, suggesting scaffold-dependent enhancement of colonization and/or metabolic activity in mixed culture, as shown in Fig. 5. Notably, the lactate levels observed in co-culture were lower than those obtained for *L. plantarum* in single-species experiments conducted in MRS-based conditions as shown in Fig. 4(a) and (b). A plausible explanation is the difference in nutrient composition between LB and MRS media used in these experiments.[28] LB is primarily composed of sodium chloride, yeast extract, and tryptone, a trypsin digest of casein, whereas MRS contains additional carbon and growth factors such as glucose and meat extract-derived nutrients and vitamins. Because lactic acid bacteria are generally more fastidious, the LB-based co-culture environment is expected to impose nutritional limitations, resulting in reduced metabolic activity and slower growth of *L. plantarum*, and consequently lower lactate accumulation compared with MRS-supported cultivation.

Across static and dynamic experiments, the villus-like scaffold enabled cultivation and quantification of bacterial colonization using imaging-based analysis, while effluent analytics (lactate and GUS activity) provided functional outputs under transport. The dynamic experiments particularly highlighted a critical analytical insight: effluent-based metrics and scaffold-localized colonization can decouple under flow, as evidenced by *E. coli* behavior where effluent signals decreased while scaffold imaging increased.

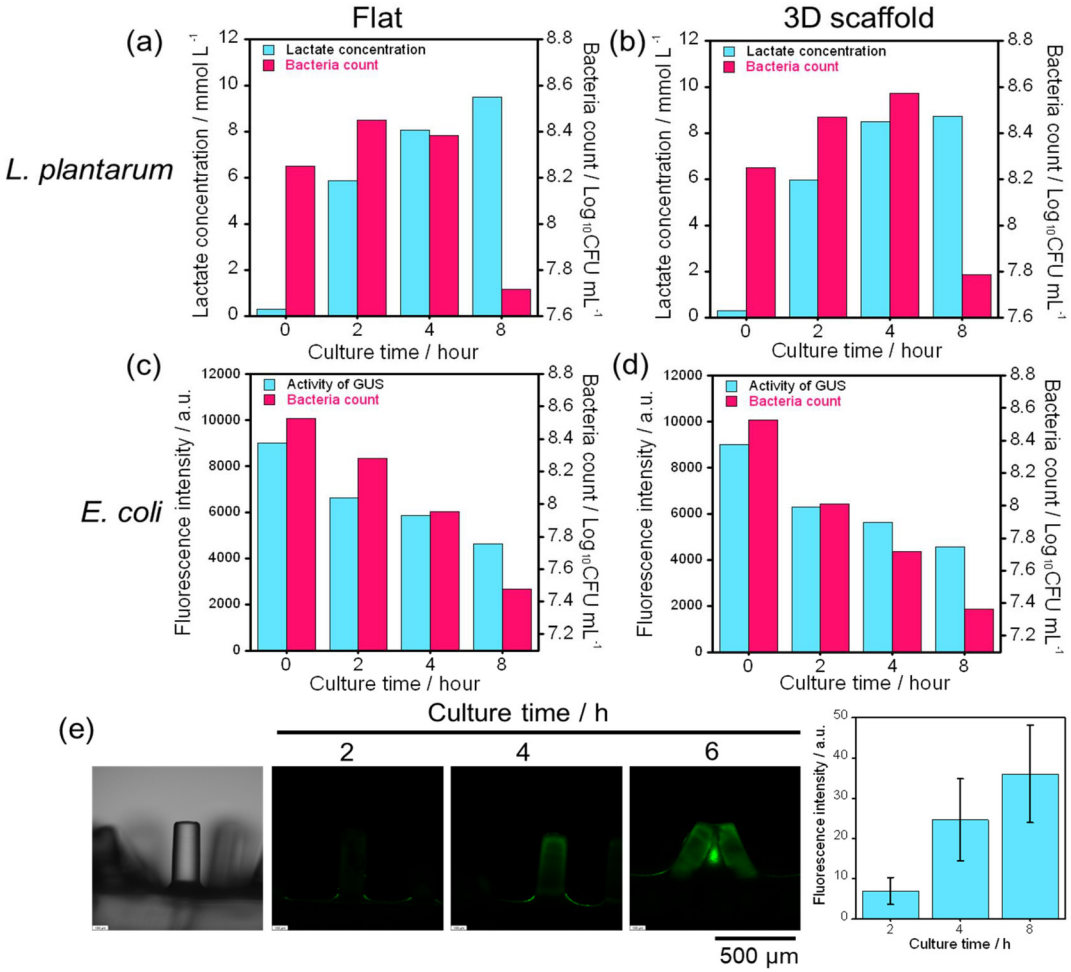

Fig. 4 Effluent analysis of *L. plantarum* (a and b) and *E. coli* (c and d) under the dynamic perfusion operation in flat (a and c) and 3D scaffold (b and d). Concentrations of lactate and fluorescence intensity of 4-methylumbelliferone produced by β-glucuronidase (GUS) digestion of the substrate, 4-methylumbelliferyl β-D-glucuronide hydrate, for quantitative measurements of *L. plantarum* and *E. coli* metabolic activities, respectively. The bacteria counts were measured by colony counting method using the collected effluent. (e) Representative cross-sectional images of the 3D hydrogel scaffold were captured by a confocal microscope at the culture time under the dynamic perfusion operation at an initial *E. coli* concentration of 10^8 CFU mL^{-1}. The right bar graph shows the fluorescence intensity of *E. coli* observed in the left images as a function of the culture time. The fluorescence intensities and error bars represent the mean and standard deviation of 4 pillar images, respectively.

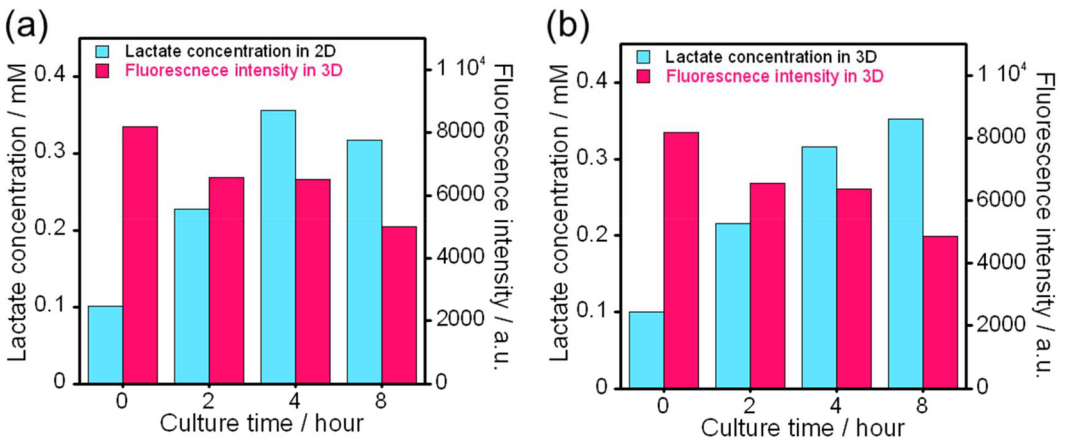

Fig. 5 Effluent analysis of co-cultured LB medium of *L. plantarum* and *E. coli* at a mixing concentration ratio of 1 : 1 under the dynamic perfusion operation. Time-courses of concentration of lactate and GUS activity in the effluents co-cultured on (a) a flat scaffold and (b) a 3D scaffold are shown.

In addition, the dynamic cultivation within the closed device is expected to become oxygen-limited, favoring fermentative energy metabolism for both facultative anaerobes, *L. plantarum* and *E. coli*. Under such conditions, interactions between the two species can further shape the lactate trajectory. In LB medium, *E. coli* can maintain growth by utilizing available nutrients and, when fermentable sugars are limited, redirecting central metabolism *via* gluconeogenic routes from non-sugar substrates. In this context, we hypothesize that *E. coli* may consume lactate produced by *L. plantarum* as a carbon source *via* conversion to pyruvate, thereby supporting its own fermentative metabolism and growth and simultaneously reducing the net lactate accumulation observed in the effluent.

Taken together, the co-culture results highlighted two important analytical implications. First, medium composition, LB or MRS, can strongly affect the apparent metabolic outputs in a dual-readout device, emphasizing the need to report and control nutrient context when comparing conditions. Second, the villus-like scaffold–integrated platform provides a device-level basis to probe interaction-dependent outcomes as production or consumption of metabolites under perfusion, thereby serving as a practical prototype for quantitative microbiota-formation studies.

Conclusions

We developed a villus-mimicking hydrogel scaffold-integrated modular microfluidic device as a next-generation analytical platform for quantitative bacterial colonization studies. The system unifies 3D microtopography, robust perfusion operation, and dual readouts combining *in situ* imaging with software-based quantification and effluent biochemical assays. Replica-molded 3D agarose scaffolds were fabricated with improved replication yield using ultrasonication-assisted bubble removal and ethanol dehydration steps. Under dynamic perfusion, the platform supported bacterial cultivation of *L. plantarum* and *E. coli* and enabled time-resolved measurement of lactate production and GUS activity. The 3D villus scaffold enhanced *L. plantarum* colonization and metabolic output relative to a flat control as well as spatially specific colonization of *E. coli*. Even under the co-culture of the two bacteria, the production of metabolites under gut-mimic flow condition suggested the complexity of the microbiota-formation process. This modular architecture and dual-readout strategy provide a scalable basis for analytical investigations of gut microbiota assembly, with potential extension to gradient control, multi-species consortia, and multiplexed metabolite profiling.

Author contributions

The manuscript was written through contributions of all authors. All authors have given approval to the final version of the manuscript. Y. Y., W. I., S. I., and N. K. designed the research, conducted the experiments and analyzed the data; N. K. wrote the paper.

Conflicts of interest

The authors declare no competing financial interest.

Data availability

The data supporting this article, including microscopy images, ImageJ-derived intensity metrics, and effluent assay datasets (lactate and β-glucuronidase activity), are available within the article and its supplementary information (SI). Supplementary information: Fig. S1 showed multicolor confocal fluorescence microscope images of *L. plantarum* and *E. coli* in co-culture on the flat scaffold; Fig. S2 showed multicolor confocal fluorescence microscope images of *L. plantarum* and *E. coli* in co-culture on the villus-like 3D scaffold; Fig. S3 showed crossover study of *E. coli* and *L. plantarum* metabolic activities. See DOI: https://doi.org/10.1039/d6an00592f.

Additional raw data are available from the corresponding author upon reasonable request. References cited in the SI are listed in the main article reference list.

Acknowledgements

The authors wish to thank Dr Yuki Okugawa, Section of Bioresource and Bioenvironmental Sciences, Center for Advanced Technical and Educational Supports, Faculty of Agriculture, Kyushu University, for her technical assistance in confocal microscope observation using TCS SP8 (Leica) as well as Dr Tatsuya Kawara, Technical division, School of Engineering, Kyushu University, for their technical assistance to fabricate an acrylic holder and an acrylic lid. This work was supported by a JSPS Grant-in-Aid for Scientific Research (B) 24K01322 and the research grant from the Mishima Kaiun Memorial Foundation.

References

1 K. J. O'Riordan, G. M. Moloney, L. Keane, G. Clarke and J. F. Cryan, *Cell Rep. Med.*, 2025, **6**, 101982.
2 Y. Han, Z. Wang, J. Xie, G. Yang, M. Su, S. Wang, M. Yang, H. Yu, M. Li, L. Wang, Y. Zhang and B. Hou, *Front. Microbiol.*, 2026, **17**, 1785607.
3 Y. Shen, N. Fan, S. Ma, X. Cheng, X. Yang and G. Wang, *MedComm*, 2025, **6**, e70168.
4 A. Safarchi, G. Al-Qadami, C. D. Tran and M. Conlon, *Front. Microbiol.*, 2025, **16**, 1559521.
5 Y. Shao, C. Garcia-Mauriño, S. Clare, N. J. R. Dawson, A. Mu, A. Adoum, K. Harcourt, J. Liu, H. P. Browne,

M. D. Stares, A. Rodger, P. Brocklehurst, N. Field and T. D. Lawley, *Nat. Microbiol.*, 2024, **9**, 2570–2582.
6 J. Ahn, E. Lkhagva, S. Jung, H. Kim, H. Chung and S. Hong, *Cell. Microbiol.*, 2023, 6868417.
7 R. An, E. Wilms, J. Gerritsen, H. K. Kim, C. S. Pérez, I. B. van der Vaartd, D. M. A. E. Jonkersc, G. T. Rijkers, W. M. de Vos, A. A. M. Mascleec, E. G. Zoetendal, F. J. Troost and H. Smidt, *Gut Microbes*, 2024, **16**, 2350173.
8 A. Kriaa, V. Mariaule, C. D. Rudder, A. Jablaoui, H. Sokol, P. Wilmes, E. Maguin and M. Rhimi, *Gut Microbes*, 2024, **16**, 2333434.
9 T. Kaden, R. Alonso-Román, J. Stallhofer, M. S. Gresnigt, B. Hube and A. S. Mosig, *Adv. Healthcare Mater.*, 2025, **14**, 2402756.
10 A. Ofori-Kwafo, I. Sigdel, E. A. Mamun, J. Zubcevic and Y. Tang, *Physiol. Rep.*, 2025, **13**, e70356.
11 A. E. Wheeler, V. Stoeger and R. M. Owens, *Lab Chip*, 2024, **24**, 1266–1292.
12 M. Ballerini, S. Galiè, P. Tyagi, C. Catozzi, H. Raji, A. Nabinejad, A. D. G. Macandog, A. Cordiale, B. I. Slivinschi, K. K. Kugiejko, M. Freisa, P. Occhetta, J. A. Wargo, P. F. Ferrucci, E. Cocorocchio, N. Segata, A. Vignati, A. Morgun, M. Deleidi, T. Manzo, M. Rasponi and L. Nezi, *Nat. Biomed. Eng.*, 2025, **9**, 967–984.
13 F. Yokoi, S. Deguchi and K. Takayama, *Regener. Ther.*, 2025, **29**, 541–550.
14 E. Delannoy, A. Burette, S. Janel, S. Poiret, N. Deboosere, C. Daniel and A. Grassart, *Lab Chip*, 2025, **25**, 4396–4409.
15 S. Abdollahi, B. Zarin, M. Vatani, F. Vajhadin, M. Hassani, P. Jalali, K. Kim and A. Sanati-Nezhad, *Nat. Commun.*, 2025, **16**, 4120.
16 I. Roegiers, T. Gheysens, M. Minsart, P. D. Clercq, K. Vanbeversluys, N. Rać, G. Stroka, J. de Croock, T. Van de Wiele, P. Dubruel and M. C. Arroyo, *Sci. Rep.*, 2025, **15**, 8214.
17 M. Sieders, P. Candry and S. El Aidy, *Microbiome*, 2025, **13**, 233.
18 X. Jin, F. B. Yu, J. Yan, A. M. Weakley, V. Dubinkina, X. Meng and K. S. Pollard, *Nat. Commun.*, 2023, **14**, 3510.
19 Y. Liu, D. Li, L. Ma, Y. Wen and D. Shi, *Front. Microbiol.*, 2025, **16**, 1561004.
20 F. Henkel and O. Lieleg, *Biomacromolecules*, 2025, **26**, 2293–2303.
21 B. C. Huck, O. Hartwig, A. Biehl, K. Schwarzkopf, C. Wagner, B. Loretz, X. Murgia and C. M. Lehr, *Biomacromolecules*, 2019, **20**, 3504–3512.
22 M. Padra, B. Adamczyk, J. Benktander, B. Flahou, E. C. Skoog, J. T. Padra, A. Smet, C. S. Jin, R. Ducatelle, T. Samuelsson, F. Haesebrouck, N. G. Karlsson, S. Teneberg and S. K. Lindén, *Virulence*, 2018, **9**, 898–918.
23 H. Lennernaäs, *J. Pharm. Sci.*, 1998, **87**, 403–410.
24 D. Shalon, R. N. Culver, J. A. Grembi, J. Folz, P. V. Treit, H. Shi, F. A. Rosenberger, L. Dethlefsen, X. Meng, E. Yaffe, A. Aranda-Díaz, P. E. Geyer, J. B. Mueller-Reif, S. Spencer, A. D. Patterson, G. Triadafilopoulos, S. P. Holmes, M. Mann, O. Fiehn, D. A. Relman and K. C. Huang, *Nature*, 2023, **617**, 581–591.
25 M. Ballerini, S. Galiè, P. Tyagi, C. Catozzi, H. Raji, A. Nabinejad, A. D. G. Macandog, A. Cordiale, B. I. Slivinschi, K. K. Kugiejko, M. Freisa, P. Occhetta, J. A. Wargo, P. F. Ferrucci, E. Cocorocchio, N. Segata, A. Vignati, A. Morgun, M. Deleidi, T. Manzo, M. Rasponi and L. Nezi, *Nat. Biomed. Eng.*, 2025, **9**, 967–984.
26 M. N. M. Shayan, Y. Tanaka, R. Hirano, Y. Nakaya and H. Satoh, *Water Res.*, 2023, **246**, 120689.
27 M. M. Abdulkadieva, E. Sysolyatina, E. V. Vasilieva, A. Gusarov, P. A. Domnin, D. A. Slonova, Y. M. Stanishevskiy, M. M. Vasiliev, O. F. Petrov and S. A. Ermolaeva, *Sci. Rep.*, 2022, **12**, 614.
28 E. J. Culp and A. L. Goodman, *Cell Host Microbe*, 2023, **31**, 485–499.